Conduction-electron spin relaxation and diffusion in the radical cation salt diperylene hexafluorophosphate

Tim Wokrina and Elmar Dormann
Physikalisches Institut, Universität Karlsruhe, Technische Hochschule, D-76128 Karlsruhe, Germany

Noam Kaplan
Racah Institute of Physics, Hebrew University, Jerusalem, Israel

(Received 28 May 1996)

Single crystals of the quasi-one-dimensional organic conductor $(PE)_2PF_6\cdot\frac{2}{3}THF$ (PE: perylene, THF: tetrahydrofurane) were studied by pulsed-electron spin resonance (ESR) at Larmor frequencies of $\nu = 300$ MHz and 10 GHz in the metallic high-temperature phase ($T>100$ K). Anisotropy and temperature dependence of conduction-electron spin-lattice and spin-spin relaxation were derived. The anisotropy of the diffusion constant exceeds a factor of 800. Quasimicroscopic restriction of the spin diffusion was analyzed by static-gradient spin-echo ESR, indicating characteristic chain lengths of ~ 90 μm. A conclusive picture of charge and spin dynamics of this molecule-based metal can thus be derived. [S0163-1829(96)06340-0]

I. INTRODUCTION

Molecule-based quasi-one-dimensional (1D) metals constructed from planar, aromatic π electron donors like fluoranthene and perylene have unique conduction electron (c.e.) properties. In particular, these c.e.'s exhibit a very long spin-lattice relaxation time, of more than 10 μs, in spite of very short scattering times of only several fs. Among other reasons, the reduced c.e. spin relaxation rate is affected by the highly one-dimensional spin and charge-carrier motion along the conducting channels of arenes.[1,2] Consequently, a step by step effort evolved since the early 80's to utilize electron-spin-resonance (ESR) methods for the study of such systems, most successfully in fluoranthene compounds.[3–9]

Currently, a rather comprehensive ESR investigation of another important quasi-1D conductor—namely, diperylene hexafluorophosphate radical cation salt[10,11]—is presented. We describe a variety of magnetic resonance measurements, including ESR, transverse and longitudinal c.e. relaxation rates, and c.e. spin diffusion measurements, under static magnetic-field gradients. These measurements, with some additional recent results,[11–14] are correlated with susceptibility, transport, and specific-heat measurements in a study of the nature of c.e. spin dynamics and c.e. motions in conducting perylene salts.

Some relevant background details concerning the perylene compounds are called for.[10,11] In this system, four perylene (PE) molecules form the periodic unit along the one-dimensional stack (crystallographic c direction), and transfer three electrons to three closed shell counter ions PF_6^-, which thus become diamagnetic. The conductive stacks are surrounded and separated by additional diamagnetic, neutral PE molecules. Tetrahydrofurane (THF) solvent molecules occupy sites between the (PE) stacks and give rise to additional disorder. The correct description of these conducting salts is thus $(PE)_4^{3+\bullet\bullet\bullet}(PE)_2(PF_6^-)_3\cdot 2$ THF, but will be abbreviated as $(PE)_2PF_6\cdot\frac{2}{3}THF$ in the following.

These salts show metallic microwave conductivity of up to 250 S/cm at room temperature (10.2 GHz), increasing with decreasing temperature.[11] Actual values depend on the individual crystal as is often the case with quasi-one-dimensional conductors. Besides the Peierls transition at $T_P=(118\pm 2)$ K, leading to a low-temperature energy gap of $2\Delta(0)\approx(68\pm 4)$ meV, an additional structural phase transition is observed in the metallic range.[11,12] Splitting of x-ray reflections indicates a reduction from monoclinic to triclinic symmetry below about 220 K, which gives rise to an increase of electrical resistivity with a lowering of the temperature. In this temperature range, THF motion slows down to below $1/\tau_c = 100$ MHz, until a second-order phase transition at $T_r=(153\pm 2)$ K results in rotation of PE stacks by several degrees around the stacking axis.[13] Finally, the extremely narrow ESR linewidth, of less than 7 mG at 120 K for $(PE)_2PF_6\cdot\frac{2}{3}THF$, points to quasi-one-dimensionality of the c.e. motion, but no clear-cut analysis of the anisotropy is available.[14]

The paper is organized as follows. Sample preparation and technical details of the experimental procedures are provided in Sec. II. The theoretical basis for the models used to analyze the results is presented in Sec. III. Additional results for c.e. spin-lattice and transverse relaxations are presented in Sec. IV A. Derivations of the anisotropy and the temperature dependence of the diffusion are presented in Secs. IV B and IV C, respectively. A derivation of the characteristic geometry of the restricted diffusive motion of the c.e in the metalic phase of our samples is presented in IV D. Finally, our main conclusions on c.e. spin dynamics, motion, and correlations with susceptibility and transport, are summarized in Sec. V.

II. EXPERIMENTAL DETAILS

A. Electrochemical crystal growth

Crystallization of $(PE)_2PF_6\cdot\frac{2}{3}THF$ was performed as described before.[10,11,14] The two different needlelike crystals used in the present investigation were labeled A and B for

distinction, where necessary. A third sample C consisted of a bundle of crystals with the stacking axis c oriented in parallel, but with arbitrary orientation of the perpendicular b directions.

B. Low-frequency pulsed ESR

Pulsed ESR at low Larmor frequency ($\nu_L = 300$ MHz) was measured on a Bruker MSL 300 NMR spectrometer, using a homebuilt probe head with saddle coil arrangement ($Q = 250$). Temperature variation was realized with an Oxford Instruments CF 1200 continuous flow cryostat. Temperature stability was better than 0.5 K. The position of the sample could be adjusted to agree with the rotation axis of the field coils. The air cooled Helmholtz coils and linear gradient coils could be rotated allowing angular-dependent experiments with 0.01° relative resolution. However, the absolute accuracy of the sample orientation was restricted to 5°, due to the small length of the crystals.

90° pulses of 0.6-μs duration were applied, but a receiver deadtime of up to 5 μs had to be allowed for. Receiver bandwidth was restricted to 2 MHz. Phase-alternated pulse and receiver cycles were generally adopted in order to minimize ringing effects and spurious baseline shifts as is the general practice in solid-state NMR.

Spin-lattice relaxation time T_1 was derived by the inversion-recovery method [$180° - \tau - 90°$ sequence] (Ref. 15) using integration of the real part of the Fourier-transformed Free conduction decay (FID) signal for the quantity to be fitted by $M_0[1 - 2\exp(-\tau/T_1)]$. The transverse relaxation time T_2 was measured using the $90° - \tau - 180° - \tau$ spin-echo sequence[15] and fitting the echo amplitude $E(2\tau)$ by the $\exp(-2\tau/T_2)$ dependence. Again, Fourier transformation and integration of the echo signal was used.

The diffusion constant was derived from the additional attenuation of the spin echo in a static field gradient G for $|G| \leqslant 0.320$ T/m,

$$E(2\tau) = E_0 \exp(-2\tau/T_2)\exp(-2/3\gamma^2 G^2 D\tau^3). \qquad (1)$$

For typical T_2 values of c.e. in $(PE)_2PF_6 \cdot \frac{2}{3}THF$, only diffusion constants of $D \geqslant 5\times10^{-8}$ m^2/s are accessible with the deadtime of the NMR spectrometer.

C. *X*-band pulsed ESR

For the analysis of restrictions to diffusion, spin-echo attenuation in static magnetic-field gradients was analyzed on a commercial electromagnet based Bruker ESP 380 spectrometer operated at 9.5 GHz.[8] For these experiments, the $90° - \tau - 90° - \tau$ echo sequence with a pulse length of 12 ns and phase cycling was used. Pulse separation was varied between 0.2 and 8 μs. Deadtime amounted to only 200 ns, thus larger gradients G could be applied than at $\nu_L = 300$ MHz. The field gradient was produced by two additional soft iron wedges located on the pole caps.[8] Gradient intensity was varied by using wedge sets of different angles. Each gradient value was determined by a one dimensional ESR projection imaging of sample B, with an accurately determined length of (2.125 ± 0.2) mm. To avoid errors caused by insufficient excitation bandwidth, the imaging measurements were performed using a field sweep technique. Gradient values of 0.292, 0.723, and 2.017 T/m were realized (10% absolute error). Orientation of the crystal's stacking axis c with respect to the direction of the magnetic-field gradient was performed by maximizing the spectral width.

III. THEORETICAL BACKGROUND

A. Spin-lattice and spin-spin relaxation

In three-dimensional metals, spin-orbit interaction governs the conduction-electron spin-lattice relaxation. According to Elliot,[16] $1/T_1$ can be estimated with

$$\left(\frac{1}{T_1}\right)_{\text{s.o.}} = \alpha\frac{(\Delta g)^2}{\tau_s}. \qquad (2)$$

α is a numerical factor of about 30, Δg the deviation of the relevant principal component of the g tensor from the free-electron value $g_e = 2.002\,32$, and τ_s the electron-phonon scattering time, also reflected in the temperature-dependent electrical conductivity. For arene molecule-based conductors like $(PE)_2PF_6 \cdot \frac{2}{3}THF$, $g_{ii} - g_e$ is small. It amounts to $+70\times10^{-5}$ and -4×10^{-5} for magnetic-field along the short and long PE molecular axes, or -7×10^{-5} for the field perpendicular to the PE molecular plane.[14] Thus the corresponding contribution to $1/T_1$ will be comparatively low. Moreover, this rate is additionally reduced by the one-dimensionality of the c.e. motion. Only scattering perpendicular to the one-dimensional stack, characterized by a scattering or hopping time constant $\tau_\perp$, results in spin-lattice relaxation, which can be estimated from[17]

$$\left(\frac{1}{T_1}\right)_{\text{s.o.}} \approx \frac{(\Delta g)^2}{\tau_\perp}. \qquad (3)$$

Thus additional contributions, caused by hyperfine interaction with the PE protons and by exchange-modulated dipolar interaction of c.e. spins with the spins of localized paramagnetic defects in the crystalline stacks, have to be considered as well.

The influence of the anisotropic hyperfine contributions to spin-lattice and spin-spin relaxation rates for magnetic-field in the z direction can be described by[18]

$$\left(\frac{1}{T_1}\right)_{\text{hf,z}} = \gamma^2(\langle\Delta B_x^2\rangle + \langle\Delta B_y^2\rangle)J(\omega_L), \qquad (4)$$

$$\left(\frac{1}{T_2}\right)_{\text{hf,z}} = \gamma^2\langle\Delta B_z^2\rangle J(0) + \frac{\gamma^2}{2}(\langle\Delta B_x^2\rangle + \langle\Delta B_y^2\rangle)J(\omega_L), \qquad (5)$$

where $\langle\Delta B_i^2\rangle$ is the second moment of appropriate component of the fluctuating hyperfine interaction. For the spectral density $J(\omega)$, the Lorentz function corresponding to the exponential decay of the correlations with time constant τ_c, i.e.,

$$J(\omega) = \frac{\tau_c}{1+\omega^2\tau_c^2}, \qquad (6)$$

was occasionally sufficient for a semiquantitative description. In order to take the quasi-one-dimensionality of the c.e. motion with scattering time constants $\tau_\parallel$ and $\tau_\perp$ into account, the spectral density

$$J(\omega)=\frac{1}{2}\left(\frac{\tau_\parallel\tau_\perp}{2}\,\frac{1+\sqrt{1+\omega^2\tau_\perp^2}}{1+\omega^2\tau_\perp^2}\right)^{1/2} \tag{7}$$

was introduced.[19] For the low-frequency limit, Eq. (7) yields

$$J(\omega\rightarrow 0)=\tfrac{1}{2}\sqrt{\tau_\parallel\tau_\perp}. \tag{8}$$

Due to the large number of protons per PE molecule, the anisotropy of the hyperfine interaction is largely averaged out, and $\langle\Delta B_{\rm hf}^2\rangle=$ 0.44, 0.41, and 0.67 $(\mathrm{mT})^2$ are obtained for fields along the short or long in-plane PE molecular axis, or normal to the molecular plane.[20]

It was shown previously that electronic spin dipolar interaction dominates the orientation, temperature, and frequency dependence of $(T_1)^{-1}$ as well as $(T_2)^{-1}$ in arene radical cation salts at least for temperatures below the Peierls transition.[14,20,21] Spectral densities corresponding to Eq. (6) proved appropriate and short correlation times τ_c resulted from fast Korringa-type relaxation of the defect spins to the c.e. spins via exchange interaction.[14,21,22] Even for the metallic range of $(\mathrm{PE})_2\mathrm{PF}_6\cdot\frac{2}{3}\mathrm{THF}$, analysis of the ESR linewidth indicated the relevant contribution of dipole dipole interaction.[14] Reasonable accuracy was obtained even when approximating the electron-spin distribution by in-stack point dipoles. Thus the respective contribution may be parametrized (with ϑ the angle of magnetic-field with respect to the stacking axis) by[14,21,22]

$$\left(\frac{1}{T_1}\right)_d=3/2d(T)\{\sin^2\vartheta\cos^2\vartheta J(\omega_L)+\sin^4\vartheta J(2\omega_L)\} \tag{9}$$

and

$$\left(\frac{1}{T_2}\right)_d=d(T)\{\tfrac{3}{8}(1-3\cos^2\vartheta)^2J(0)+\tfrac{15}{4}\sin^2\vartheta\cos^2\vartheta J(\omega_L)+\tfrac{3}{8}\sin^4\vartheta J(2\omega_L)\}. \tag{10}$$

Here $d=(3\gamma^4\hbar^2/2R^6)P$ characterizes the interaction strength, and is constant in the metallic range. It depends on the closest separation of defect and conduction electron spins, R, and the probability P to encounter a defect spin (defect concentration).

B. Anisotropic diffusion of the conduction-electron spins

For unrestricted diffusion in an isotropic system with static magnetic-field gradient G, the spin echo decays according to Eq. (1), as was already derived by Torrey.[23] Here D is the microscopic diffusion constant of the spins. In the present investigation, the magnetic-field gradient was always applied parallel to the direction of the main field B_0,

$$B_z(z)=B_0+Gz. \tag{11}$$

For the c.e. spins in $(\mathrm{PE})_2\mathrm{PF}_6\cdot\frac{2}{3}\mathrm{THF}$ single crystals with monoclinic symmetry, diffusion is highly anisotropic. $D_\parallel$, the largest principle value of the D tensor, is observed for the field gradient oriented along the stacking axis c. For rotation of the crystal around an axis perpendicular to c, D of Eq. (1) can be replaced by[4]

$$D(\vartheta)=D_\parallel\cos^2\vartheta+D_\perp\sin^2\vartheta, \tag{12}$$

with ϑ the angle of B_z with respect to the c axis. Relatively small variation of $D_\perp(\varphi)$ with φ in the plane perpendicular to c is expected. $D_\perp(\varphi)$ can be determined with better accuracy by measurements and data analysis, in accord with Eq. (12) for fixed values of φ, because otherwise minor misadjustment of the nominally perpendicular plane results in huge relative errors of $D_\perp(\varphi)$ due to the preponderant size of $D_\parallel$.

C. Restricted diffusion of the conduction-electron spins

The assumption of anisotropic free diffusion of the c.e. spins is only a first approximation for a real quasi-one-dimensional conductor. The low-temperature Curie tail of the static magnetic susceptibility reveals a typical defect spin concentration of about 1–2 $\times10^{-3}$ per formular unit of $(\mathrm{PE})_2\mathrm{PF}_6\cdot\frac{2}{3}\mathrm{THF}$.[11] Furthermore, low-temperature ESR allows us to identify intrastack radical spin defects and their interaction with thermally activated c.e. spins.[14,20] Thus the one-dimensional motion will be restricted by isolated defects in the stack. More importantly, extended microcracks or grain boundaries will present severe obstacles to diffusive motion even in spite of the finite transversal hopping motion.

It was shown recently for fluoranthene radical cation salts, that detailed information concerning the permeability and the relaxation effects of boundaries on the electron-spin motion can only be obtained by a careful PULSED-GRADIENT spin-echo ESR analysis.[9,24] With the simplifying assumption of reflecting, nonrelaxing walls, and assuming an exponential distribution of stack lengths l_s given by

$$P(l_s)=\hat{l}_s^{\,-1}\exp(-l_s/\hat{l}_s), \tag{13}$$

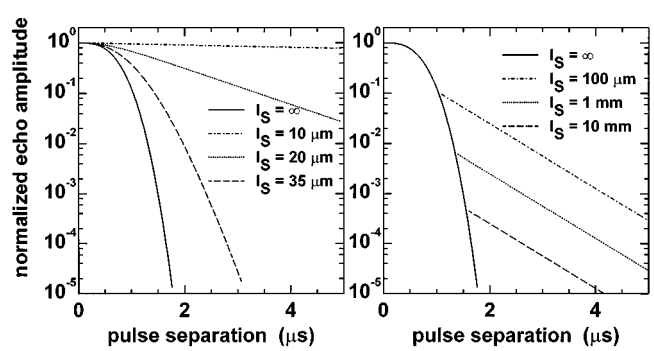

FIG. 1. ESR spin-echo attenuation for static field gradient G = 1 T/m and diffusion constant $D=1\times10^{-4}$ m^2/s (transversal relaxation divided out). Deviation from the free (unrestricted) diffusion according to the Neuman-relation [Eqs. (15) and (16)] is shown on the left. Reduced attenuation for longer chains in the ''localization regime'' (see text for details) is shown on the right.

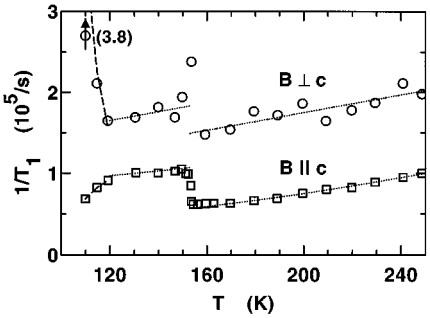

FIG. 2. Temperature dependence of the c.e. spin-lattice relaxation rate of $(PE)_2PF_6\cdot\frac{2}{3}THF$ sample C for $\nu_L = 300$ MHz and magnetic field parallel or perpendicular to the stacking axis c. The phase transitions at $T_r=(153\pm2)$ K and $T_P=(118\pm2)$ K are visible. The broken line fits are explained in text.

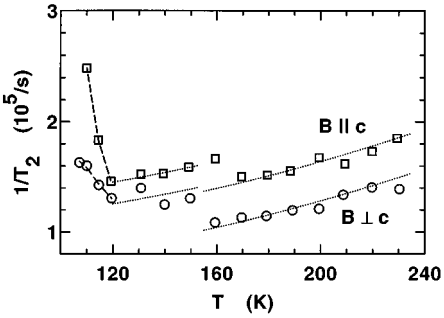

FIG. 3. Temperature dependence of the c.e. transverse relaxation rate of $(PE)_2PF_6\cdot\frac{2}{3}THF$ sample C for $\nu_L = 300$ MHz and magnetic fields parallel or perpendicular to the stacking axis c. The broken lines are a guide to the eye.

the chain length parameter $\hat{l}_s$ defining the normalized probability function

$$p(l_s)=\hat{l}_s^{-2}l_s\exp(-l_s/\hat{l}_s) \tag{14}$$

can be derived also from the spin-echo attenuation in the STATIC magnetic-field gradient.[7–9]

For the short-time behavior of the echo attenuation, Eq. (1) gives the correct description. For longer times but very short chains, the influence of the field gradient is reduced because of motional averaging. Thus a simple exponential echo decay results for large pulse separations, as is shown for typical values of the parameters and chain lengths in Fig. 1. For this figure the theoretical model of Neuman[25] and Robertson[26] is used. The model is based on an analytical solution interpolating between short- and long-time behavior, assuming a Gaussian phase distribution. The echo decay predicted by the model is given by

$$E(2\tau)=E_0\exp\left\{-2\tau/T_2-\frac{8\gamma^2G^2l_s^4}{D\pi^6}\sum_{n=0}^{\infty}\frac{1}{(2n+1)^6}\times\left(2\tau-\frac{3-4e^{-Q\tau}+e^{-2Q\tau}}{Q}\right)\right\}, \tag{15}$$

with

$$Q=D\frac{(2n+1)^2\pi^2}{l_s^2}. \tag{16}$$

Especially for large gradients G, echo decay for longer chains according to Eq. (1) would be rather fast. It was reported recently[27–29] that, in such cases, the remaining signal originates predominantly from spins residing close to the walls (''localization regime''). Dividing out T_2 effects, the long-time attenuation in that regime is given by[28]

$$E(2\tau)=E_0\frac{c}{l_s}\left(\frac{D}{\gamma G}\right)^{1/3}\exp\{-a_1D^{1/3}\gamma^{2/3}G^{2/3}\tau\}, \tag{17}$$

with $c = 5.8841$ and $a_1 = 1.0188$. The respective short- and long-time behavior is demonstrated in Fig. 1. For the convolution with the chain length distribution [Eq. (14)], the ''change over'' between short chain ''motional averaging'' [Eqs. (15) and (16)] and long chain, large gradient ''signal localization'' was chosen at $l_s=(D/\gamma G)^{1/3}$.

IV. RESULTS

A. Spin-lattice and transverse relaxation

The temperature dependence of the spin-lattice and transverse relaxation rates for the c.e. in the metallic phase of $(PE)_2PF_6\cdot\frac{2}{3}THF$ is presented in Figs. 2 and 3, respectively. It was derived at $\nu_L = 300$ MHz for magnetic-field parallel and perpendicular to the stacking axis.

Considerable continuous variation is observed at the Peierls transition $T_P=(118\pm2)$ K, most pronounced for $1/T_1(B\perp c)$ and $1/T_2(B\|c)$. Steplike anomalies at $T_r=(153\pm2)$ K accompany the structural transition, which involves rotation of PE stacks in the low-temperature phase.[14] As is typical for a relevant contribution of dipole-

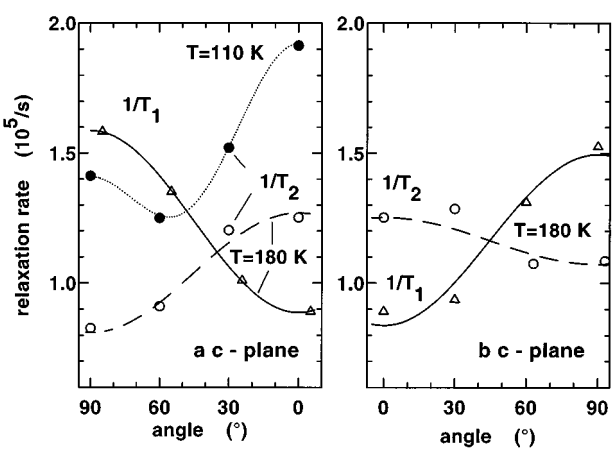

FIG. 4. Angular variation of spin-lattice and transverse relaxation rates for $(PE)_2PF_6\cdot\frac{2}{3}THF$ (sample B) for $\nu_L = 300$ MHz and $T = 180$ K. (0° is parallel to stacking axis c.) The fit curves are explained in the text. For comparison, the angular dependence of $1/T_2$ is included for a temperature below $T_P(T = 110$ K), demonstrating the predominance of the secular contribution in Eq. (10) for increasing τ_c.

TABLE I. Fit parameters for temperature dependence of spin-lattice relaxation rate [Eq. (18)].

	r_0 (10^4 s^{-1})	r_1 (s^{-1} K^{-1})	r_2 (s^{-1} K^{-2})
$B\|c, T>T_r$	3.1	≈ 0	1.10
$B\|c, T<T_r$	8.1	≈ 0	1.1
$B_\perp c, T>T_r$	6.5	549	≈ 0
$B_\perp c, T<T_r$	9.9	549	≈ 0

dipole interaction, Eqs. (9) and (10), $1/T_1$ is larger for field perpendicular to the stacking axis c than for the parallel orientation, whereas this sequence is inverted for $1/T_2$. The broken lines describing the $1/T_1$ data correspond to the relation

$$1/T_1 = r_0 + r_1 T + r_2 T^2, \tag{18}$$

and the parameters r_i are collected in Table I.

A more detailed picture of the relaxation behavior is obtained by an orientational analysis[21,22] at fixed temperature $T = 180$ K for two orthogonal planes, as is shown in Fig. 4. In order to render the fitting procedure unique, only the dipolar contribution [Eqs. (9) and (10) for $\omega\tau \ll 1$, i.e., $J(0) = J(\omega_L) = J(2\omega_L) = \tau_c$], supplemented by an angular independent part $(1/T_i)_0$, was taken into account. For comparison, the angular dependence of $1/T_2$ for $T = 110$ K, i.e., 8 K below the Peierls transition, is also included. Here, due to the larger correlation time $\omega\tau_c > 1$, the secular contribution of Eq. (10) predominates, and results in the typical magic angle minimum at $\vartheta = 54.74°$. The fitting parameters are collected in Table II.

In the metallic phase of $(PE)_2PF_6 \cdot \frac{2}{3}THF$, there is only minor variation of $1/T_1$ in the plane perpendicular to the stacking axis c, but $1/T_2$ varies by about 30%. Interestingly, in the plane $B \perp c$, $1/T_1$ is considerably larger than $1/T_2$, indicative of very anisotropic spin dynamics. Actually, for B parallel to a^*, i.e., perpendicular to c and b, $(T_1)^{-1} \approx 2(T_2)^{-1}$, the maximum value allowed by Eqs. (4) and (5) for a vanishing secular contribution.

Of all relaxation rates, the spin-lattice relaxation rate $1/T_1$ for field parallel to the stacking axis c shows the most prominent variation around T_r, the temperature of the second-order phase transition, resulting in reorientation of the PE molecular stacks. It increases by 80% below T_r for sample B. A more detailed analysis of the angular variation for the bundle of crystals, sample C, reveals that the increase of the isotropic part of $1/T_1$ by 70% is accompanied by with a reduction of the anisotropic term by 30%.

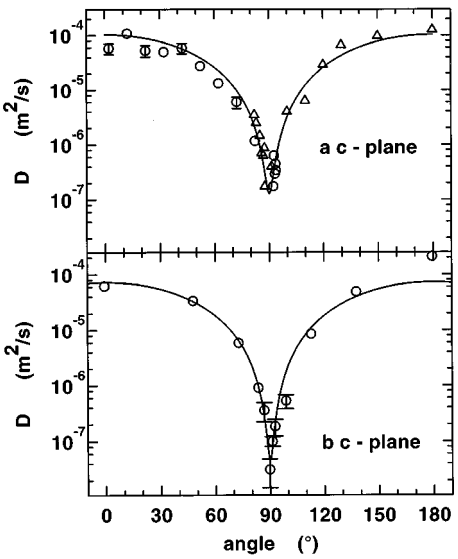

FIG. 5. Anisotropy of the diffusion constant derived by static-gradient spin-echo ESR at $\nu_L = 300$ MHz and $T = 180$ K for $(PE)_2PF_6 \cdot \frac{2}{3}THF$ (sample B) in the two orthogonal symmetry planes. Two independent measurements for the (a,c) plane are superimposed. The solid lines are the fits to Eq. (12) with parameters compiled in Table III.

B. Anisotropy of the diffusion constant

The anisotropy of the c.e. spin diffusion was analyzed by static gradient pulsed ESR for the same sample B at $\nu_L = 300$ MHz, again at $T = 180$ K. The variation of $D(\vartheta)$ in the two symmetry planes of the monoclinic structure containing the stacking axis c is shown in Fig. 5, together with a fit to Eq. (12), that evidently gives a very reasonable description of the angular dependence. The corresponding main values of the D tensor are collected in Table III. The small value of $D_\perp(\|b)$ is within the error limit of the current analysis, resulting in a very large lower limit of $D_c/D_b \geqslant 1500$ for the anisotropy in the bc plane. Even in the ac plane, an anisotropy of about 800:1 is manifested. The two values of $D_\|$, i.e., the values of the fitted curves at $\vartheta = 0$ or 180°, should be identical, and the difference reflects the accuracy of the present analysis.

C. Temperature dependence of the diffusion constant

The temperature dependence of the diffusion constant $D_\|$ is plotted in Fig. 6. For comparison, on identical scales, the temperature dependence of the microwave conductivity

TABLE II. Parameters characterizing the angular dependence of relaxation rates [Eqs. (9) and (10)].

Sample	Rate	Rotation plane	T (K)	$(T_i)_0^{-1}$ (10^4 s^{-1})	$d\tau_c$ (10^4 s^{-1})
B	$1/T_1$	(ac)	180	8.87	2.33
B	$1/T_1$	(bc)	180	8.38	2.19
B	$1/T_2$	(ac)	180	3.52	3.11
B	$1/T_2$	(bc)	180	8.92	1.20
B	$1/T_2$	(ac)	110	12.37	2.27
C	$1/T_1$	average	170	5.94	2.69
C	$1/T_1$	average	147	10.01	1.86

TABLE III. Anisotropy of spin diffusion constant for $(PE)_2PF_6\cdot\frac{2}{3}THF$, sample B, at $T=180$ K.

Rotation plane	$D_\parallel$ (10^{-4} m^2 s^{-1})	$D_\perp$ (10^{-7} m^2 s^{-1})	anisotropy $D_\parallel/D_\perp$
(ac)	(1.01 ± 0.30)	(1.28 ± 0.49)	790 ± 330
(bc)	(0.73 ± 0.22)	$\leqslant(0.47 \pm 0.15)$	$\geqslant 1550 \pm 650$

(10.2 GHz) parallel to the c axis,[11] and the paramagnetic susceptibility, are also given. Two data sets are shown for the latter quantity: the results of a static susceptibility measurement, corrected for diamagnetic and Curie-paramagnetic defect contributions[11] and (on relative scale) the results of the ESR intensity variation.[14] There is no indication for a frequency dependence of $D_\parallel$. However, the diffusion for the bundle of crystals, sample C, is smaller by a factor of 2 than that of the individual single crystal, sample B, outside the measuring error bar of about 30%. This is in accord with an earlier observation of sample-dependent electrical conductivity, reflecting the influence of sample defects on carrier motion in highly one-dimensional conductors. More information on restriction to the one-dimensional motion can be obtained from a analysis of the echo attenuation up to the long-time regime, as detailed in Sec. IV D. It is of interest to note that $D_\parallel$ shows only minor variations through the Peierls transition $T_P=(118\pm2)$ K, whereas static susceptibility and microwave conductivity decrease by an order of magnitude by the time $T=100$ K.

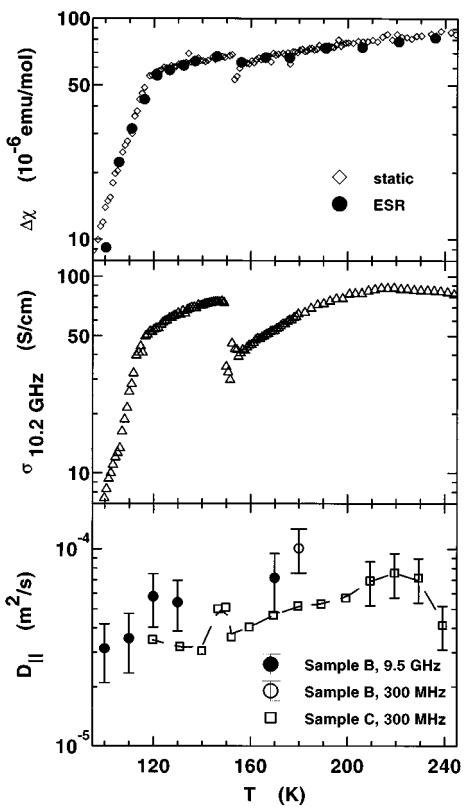

FIG. 6. Temperature dependence of c.e. properties for $(PE)_2PF_6\cdot\frac{2}{3}THF$. The magnetic susceptibility (Ref. 11) shown on top was obtained after correcting for a diamagnetic and a Curie-paramagnetic defect contribution. ESR intensity variation (relative units) is also included (Ref. 14). Microwave conductivity parallel to the stacking direction was measured at 10.2 GHz (Ref. 11). Diffusion constants $D_\parallel$ for one individual crystal (B) and a bundle of crystals (C) is presented for two measuring frequencies (300 MHz, 9.5 GHz). The Peierls transition at $T_P=118$ K, and structural transitions at $T_r = 153$ K and $T_{\text{tric.}}\leqslant 220$ K can be distinguished.

D. Restricted diffusion in $(PE)_2PF_6\cdot\frac{2}{3}THF$

As discussed in Sec. III C, ESR spin-echo attenuation in static field gradients must be monitored along the widest possible time range in order to determine the influence of restrictions on the diffusion. To achieve a dynamic range of four orders of magnitude, these measurements were performed at $\nu_L = 9.5$ GHz.

Figure 7 depicts results for $T = 130$ and 170 K, below and above the structural transition at $T_r = 153$ K. The bending over from fast short-time decay, typical of free diffusional motion of all the c.e. spins in the crystal, to slower exponential decay at a later time is clearly noticeable. In the long-time regime, the signal is dominated by the relatively small number of c.e. spins in very short chain segments. The solid lines in Figs. 7(a), and 7(b) show the fits to the theoretical model of Neuman [Eq. (15)]. For the fits in Figs. 7(c) and 7(d) the relations considering the ''localization regime''[28] were taken into account, as explained in Sec. III C [Eq. (14)–(17)]. The parameters deduced from the fits for the individual gradient values and their averages are compiled in Table IV. Transverse relaxation was taken into account, and the T_2 values deduced with Eqs. (14)–(17) for $\nu_L = 9.5$ GHz agree reasonably with those derived at $\nu_L = 300$ MHz, e.g., $T_{2,\parallel}=7.8$ μs at 180 K. There is adequate agreement of the $D_\parallel$ values derived with the two different models. The $D_\parallel$ values derived from the fit with Eqs. (14) and (15) are in fact those included in Fig. 6. For the chain-length distribution function [Eqs. (13) and (14)], a characteristic chain length $\hat{l}_s$ of about 90 μ m is obtained with the Neuman model, quite comparable to the value derived with the same model for fluoranthene radical cation salts.[8] The smaller diffusion constant $D_\parallel$ of the perylene salt changes the echo attenuation in a rather pronounced fashion, however, as is visible by comparing Fig. 7 with Fig. 1 of Ref. 8.

On a visual inspection, both models describe the observed echo attenuation rather well. For the lowest gradient, there is also no clear discrimination by the χ^2 fits. For the two larger gradients, the Neuman model gives superior χ^2 fits (e.g., by up to a factor of 2 for $T = 170$ K and $G = 2.017$ T/m). There are systematic differences between the fit values obtained with the two different models. The values of $\hat{l}_s$ and $T_{2,\parallel}$ obtained with the Neuman model [Eqs. (14) and (15)] are smaller, and the $D_\parallel$ values are slightly larger than those obtained with the extended model that considers also the spins in the''localization regime.''[27–29] Especially for the latter model, a systematic increase of T_2 and decrease of $\hat{l}_s$ with

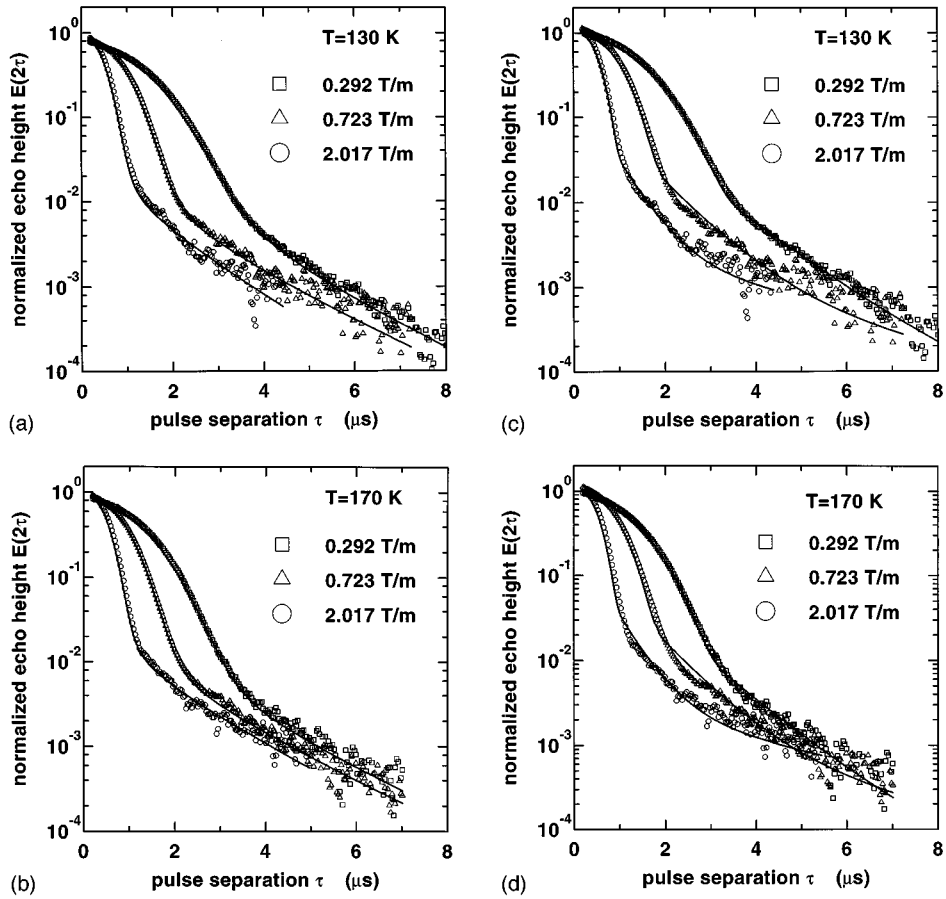

FIG. 7. ESR spin-echo attenuation for $(PE)_2PF_6\cdot\frac{2}{3}THF$ as a function of pulse separation at three gradient intensities for $B\|c$ at $T = 130$ K (A) and (C) and $T = 170$ K (B) and (D). The solid-line fits according to Eqs. (14) and (15) (A) and (B) or (14)–(17) (C) and (D) are explained in the text. Parameters are compiled in Table IV.

increasing value of the gradient is observed. Furthermore, we note that fits with the Neumann model [Eqs. (14) and (15)] give T_2 values that are shorter than those obtained from fits with Eqs. (14)–(17) and also shorter than the values derived experimentally without applied gradient. This results apparently from the long-time behavior of the echo signal for pulse separation τ larger than 2 μs, which is dominated by spins in very short chains. All of the above systematic differences may indicate that the assumption of reflecting, nonrelaxing, impermeable restrictions — an assumption implying a unique T_2 throughout the sample — may not be completely valid. For example, one may expect that c.e.'s are susceptible to additional relaxation near paramagnetic defects at the ends of restricted chains (dipolar and exchange interactions,[14]) which would lead to an l-dependent T_2 mechanism. As suggested previously,[9] detailed pulsed-gradient spin-echo ESR (PGSE-ESR) experiments, and analysis might shed additional light on these systematic variations.

If the fine details of the spin-echo attenuation are considered, the ''localization'' model appears superior around $\tau = 1\,\mu$s for the largest gradient data. On the other hand, the

TABLE IV. Parameters describing restricted diffusion in $(PE)_2PF_6\cdot\frac{2}{3}THF$ (sample B), derived by static gradient spin-echo ESR (9.5 GHz, Fig. 7).

		Fit with Eqs. (14) and (15)			Fit with Eqs. (14), (15) and (17)		
T (K)	G (T/m)	$T_{2,\|}$ (μs)	$D_\|$ (10^{-4}m^2/s)	$\hat{l}_s$(μm)	$T_{2,\|}$(μs)	$D_\|$(10^{-4}m^2/s)	$\hat{l}_s$ (μm)
130	0.292	3.46	0.670	96.7	5.12	0.561	279
130	0.723	3.69	0.631	87.8	7.61	0.540	208
130	2.017	3.02	0.570	53.9	11.49	0.459	126
130	average	3.39 ± 0.34	0.624 ± 0.050	79.5 ± 22.6	8.07 ± 3.21	0.520 ± 0.054	204 ± 77
170	0.292	3.83	0.914	141	4.69	0.754	326
170	0.723	3.82	0.633	94.8	7.26	0.598	212
170	2.017	3.54	0.557	56.0	10.3	0.48	113
170	average	3.73 ± 0.16	0.701 ± 0.188	97.3 ± 42.6	7.41 ± 2.81	0.611 ± 0.137	217 ± 107

same model is clearly inferior in fitting the 2 μs $\leqslant \tau \leqslant$ 3.5 μs data for intermediate gradients.

Comparing the gradient-averaged values of $\hat{l}_s$ at 170 and 130 K, i.e., above and below the second-order structural phase transition at T_r, that leads to rotation of PE stacks around the stacking axis by small angles in opposite directions in the same crystal, we observe only a minor difference within the quoted error of the current analysis. We may thus exclude the possibility that each stack is divided in two or more noncommunicating parts as we pass through the transition. This exclusion leads to a rather significant conclusion concerning the nature of the structural transition at T_r. It implies that the molecules within individual stacks, defined already above the transition by the restrictions, must rotate in unison at least within each stack, and possibly even within domains containing more than one restricted stack. The small reduction $\hat{l}_s$ (130 K)/ $\hat{l}_s$(170 K) = 0.86 ± 0.15 [Eqs. (14) and (15)] or 0.98 ± 0.13 Eqs. 14–17 deduced by relating only $\hat{l}_s$ pair values derived for the same gradient strength, indicates that only rare exceptions exist to this rule.

V. CONCLUSIONS

A. Spin and carrier motion — diffusion anisotropy and scattering rates

The ESR data derived above can be used for a detailed picture of spin and carrier motion in $(PE)_2PF_6\cdot\frac{2}{3}THF$. In the simplified free-electron-gas picture,[30,31] the mean free path λ of the c.e. is given by

$$\lambda = v_F \tau_s , \tag{19}$$

the mobility μ of the charge carriers is given by

$$\mu = \frac{e}{m^*}\tau_s , \tag{20}$$

and the electrical conductivity σ is given by

$$\sigma = \left(\frac{N}{V}\right)\frac{e^2}{m^*}\tau_s = \left(\frac{N}{V}\right)e\mu, \tag{21}$$

where v_F is the Fermi velocity, (N/V) the carrier density and τ_s the scattering time relevant for conductivity. Since there are no indications for a decoupling of charge and spin degrees of freedom in this Peierls system, the scattering time $\tau_\parallel$, derived from the diffusion constant $D_\parallel$ by the relation

$$D_\parallel = \lambda^2/\tau_\parallel = v_F^2 \tau_\parallel , \tag{22}$$

can be identified with τ_s. Taking the ''tetramerization'' into account,[11] i.e., considering a half-filled upper band with $k_F = \pi/2c$ and $v_F = 1.32\times 10^5$ m/s, the value $D_\parallel = 1.01\times 10^{-4}$m^2/s of sample B at T = 180 K yields

$$\tau_\parallel = 5.8\times 10^{-15}\ \text{s}, \quad \lambda = 7.7\ \text{Å}.$$

This estimate is in accord with earlier results for fluoranthene radical cation salts which also indicated rather short scattering times for motion along the stacking direction with mean free paths barely surpassing intermolecular separations.[2] If the free-electron mass is used for m^* in Eq. (20), a mobility $\mu = 1.02\times 10^{-3}$m^2/V s and an electrical conductivity of $\sigma = 6.85\times 10^4$S/m is estimated from Eq. (21), in reasonable agreement with the experimental observation. The σ value was derived considering only the carrier density $(N/V) = 4.19\times 10^{26}$ m^{-3}, corresponding to the upper conduction band.[11]

In contrast to the motion of the c.e. along the stacking direction, that can be considered ''coherent,'' a hopping-type description seems more appropriate for the transversal direction, i.e.,

$$D_\perp = d^2/\tau_\perp , \tag{23}$$

with the relevant interstack separation d and a hopping rate $1/\tau_\perp$. Experimentally, only an upper limit for $D_\perp$ could be deduced, because one may not exclude a mosaiclike structure that introduces small but nonvanishing $D_\parallel$ components into the $D_\perp$ analysis.

For the shorter ''a'' separation, and using $D_\perp \leqslant 1.28\times 10^{-7}$m^2/s (Table III) and $d = a = 13.076$ Å, the estimate

$$\tau_\perp(a) \geqslant 1.34\times 10^{-11}\ \text{s}$$

is derived. Using $D_\perp \leqslant 0.47\times 10^{-7}$ m^2/s and $d = b = 14.159$ Å, one finds

$$\tau_\perp(b) \geqslant 4.27\times 10^{-11}\ \text{s},$$

i.e., more than a factor of 2300 or 7350 larger than $\tau_\parallel$. Thus perylene radical cation salts of the composition $(PE)_2PF_6\cdot\frac{2}{3}THF$ clearly merit the denotation ''quasi one-dimensional'' conductors.

B. Spin dynamics

The estimate of $\tau_\parallel = 5.8\times 10^{-15}$ and $\tau_\perp \geqslant 1.34\cdot 10^{-11}$ s for T = 180 K can be used for the quantitative interpretation of the spin-lattice and transverse relaxation rates in $(PE)_2PF_6\cdot\frac{2}{3}THF$ (Fig. 4). From Eqs. (3) and (4), the estimate $(1/T_1)_{\text{s.o.}} \leqslant 0.049, 3.69$, and 3.67×10^4s^{-1} is obtained for T = 180 K and magnetic field in a^*, b, or c direction. Thus the Elliot mechanism may explain half of the spin-lattice relaxation rate for a field parallel to the stacking direction, i.e., the orientation of vanishing dipolar contribution [Eq. (9)]. The other half ought to be caused by hyperfine interaction, requiring $J(\omega_L) \approx 1.7\times 10^{-12}$ s in order to give $(1/T_1)_{\text{hf,c}} \approx 4.5\times 10^4$ s^{-1} from Eq. (4), somewhat larger than the estimate from Eq. (8). For the other two field directions, the hyperfine contribution to $1/T_1$ should be larger by about 30%. More importantly, the dipolar contribution to $1/T_1$ has to be included, almost doubling the overall rate for a field perpendicular to c. Thus, qualitatively, all three contributions to $1/T_1$ are of comparable magnitude. Specifically, we find (s.o.):(hf):(dip) $\approx$4:4.5:0 for $B\|c$, and 4:6:6 for $B\|b$ and 0:6:6 for $B\|a^*$, all in units of 10^4 s^{-1}.

For the transverse relaxation rate, the hyperfine contribution should be even more isotropic, with the largest value (by 10 – 15 %) for field along c. The dipolar contribution should exhibit a 2:1 anisotropy with the largest value for $B\|c$, identical to the $1/T_1(B\|b)$ value. In keeping with Eq. (5), only half of the spin-orbit contributions should be felt in the T_2

measurement. Thus the $1/T_2$ contributions should add up like (s.o.):(hf):(dip) $\approx 2:6:6$ for $B \| c$, 2:5:3 for $B \| b$, and 0:5:3 for $B \| a^*$, all in unit of 10^4 s^{-1}. This sequence of the transverse relaxation rates is in general agreement with experimental observation, Fig. 4. In particular, the decomposition proposed here explains the unusual observation that, for $B \perp c$, spin-lattice relaxation rate amounts to roughly twice the transverse relaxation rate.

We will now consider the temperature dependence of the T_2 relaxation. We showed recently[14] that the correlation time τ_c, and proportionally $d\tau_c$ for the electron-spin dipole-dipole contribution varies like $(\chi^2_{\text{c.e.}}T)^{-1}$ in the range $T > 90$ K for $(PE)_2PF_6 \cdot \frac{2}{3}THF$. Thus for temperatures lower than $T = 180$ K, due to decreasing T, and $\chi_{\text{c.e.}}(T)$ (Fig. 6), τ_c, and $d\tau_c$ increase. This leads to suppression of the non-secular contributions in $(1/T_2)_d$ in Eq. (10). The predominance of the $(1-3\cos^2\vartheta)^2$ part for $T = 110$ K is thus explained (Fig. 4). Especially below $T_P = 118$ K, $1/T_2$ must (and does) increase due to further increase of τ. The spin dynamics in the low-temperature phase was analyzed previously.[14]

The temperature dependence of spin-orbit and hyperfine contributions should also be considered. Figure 6 indicates that $D_\parallel$, and thus $\tau_\parallel$, increase weakly with temperature from 100 to 220 K, except perhaps for the range close to $T_r = 153$ K. Thus a small increase of the dominating hyperfine contribution to $1/T_1$ and $1/T_2$ with temperature is to be expected, and is indeed noticeable in Figs. 2 and 3 at least for $T > T_r$.

There is one observation left to explain: Almost all relaxation rates in Figs. 2 and 3 increase, when the temperature is lowered through the structural phase transition at $T_r = 153$ K. The variation is most pronounced for the spin-lattice relaxation rate for B applied parallel to the stacking axis c. This anomaly must be due to an increase of the spin-orbit contribution, Eq. (3), below T_r. Indeed, according to the above decomposition, for $T = 180$ K the spin-orbit contribution amounts to about 50% of $1/T_1$ for $B \| c$, but to only about 11 – 14 % for all the other relaxation rates plotted in Figs. 2 and 3. Why should the spin-orbit contribution increase? Equation (3) provides the answer: Below this phase transition at T_r, $\tau_\perp$ must be reduced by almost a factor of 2 compared to the high-temperature range. This seems not unreasonable on account of the slowed-down motion of the partially disordered THF molecules, which precedes this transition. Thus $(PE)_2PF_6 \cdot \frac{2}{3}THF$ in the low-temperature ''metallic'' phase at $T_P < T < T_r$ must be less anisotropic (or less ''one dimensional'') than in the phase above T_r. This is not unexpected, because the three-dimensional Peierls distortion actually occurs starting from this phase, and the Peierls transition of $(PE)_2PF_6 \cdot \frac{2}{3}THF$ was already classified as typical of a strongly fluctuating material fitting in a quasi-three-dimensional model.[11] The doubling of the spin-orbit contribution may explain also the observed reduced anisotropy of $1/T_1$ for $T < T_r$ compared to $T > T_r$ (Sec. IV A and Table II, bundle of crystals).

C. Magnetic-resonance information on electrical conductivity

We have shown that a detailed picture of the processes contributing to electrical conductivity can be derived by a pulsed c.e. ESR analysis. For the temperature range below the Peierls transition at $T_P = 118$ K, Fig. 6 demonstrates that the mobility — reflected by the diffusion constant $D_\parallel$—has only a weak variation, whereas the charge and spin concentrations—reflected by the magnetic susceptibility — decrease by an order of magnitude within 15 K. This indicates that the decrease of the electrical conductivity below $T_P = 118$ K is dominated by the influence of the carrier concentration. This was also concluded for fluoranthene radical cation salts[32] from a theoretical analysis of the electrical conductivity.

In the temperature range $T > T_P$, the c.e. susceptibility increases slowly with temperature (Fig. 6). This is currently explained as a consequence of a pseudogap resulting from fluctuations announcing the Peierls (charge-density-wave) transition in the high-temperature phase.[11] In this temperature range, the electrical conductivity therefore rises slowly due to the smooth variation of the mobility [reflected by the diffusion constant $D_\parallel(T)$].

At $T_r = 153$ K, anisotropy of the scattering rates, i.e., $\tau_\parallel^{-1} : \tau_\perp^{-1}$ seems to be increased by about a factor of 2 to values above 2000 (Sec. V A). Thus the $(PE)_2PF_6 \cdot \frac{2}{3}THF$ crystals are more pronounced quasi-one-dimensional conductors above T_r than below it. Any restriction of diffusive c.e. motion parallel to the stacking direction is therefore difficult to bypass. Assuming an exponential distribution of chain lengths, a characteristic length $\hat{l}_s$ of about 90 μm (incorporating the largest portion of the spins) was derived comparing the observed echo attenuation with predictions of the Neuman model. There is no remarkable difference between the $\hat{l}_s$ or the $D_\parallel$ values above or below T_r. Thus the evident reduction of the macroscopic microwave electrical conductivity at $T \geqslant T_r$ (Fig. 6) seems to be linked with the reduction of the transverse hopping rate $\tau_\perp^{-1}$.

Above $T_{\text{tric}} \approx 220$ K, static susceptibility continues to increase, but electrical conductivity decreases like in classical metals due to increased scattering of the conduction electrons. This reduction of the mean free path is also reflected in the variation of $D_\parallel$.

With the static field gradient pulsed-ESR technique utilized in the present investigation, the potential of magnetic resonance has not yet been fully exploited for the purpose of obtaining detailed information on the actual restrictions to low-dimensional motion of c.e. spins in quasi-one-dimensional conductors. It appears that a pulsed magnetic field gradient analysis has to be performed in order to gain closer insight into the real chain length distribution in this ''real'' molecule-based metal.

ACKNOWLEDGMENTS

We thank R. Ruf for discussions, J. Gmeiner, D. Schweitzer, and W. Wendl for advice and assistance in crystal growth and P. Pfundstein for scanning electron microscope analysis of the crystals. We are indebted to Dr. P. Höfer, and Bruker Karlsruhe, for the opportunity to perform pulsed ESR measurements at 10 GHz. This work was supported by the Deutsche Forschungsgemeinschaft within the Sonderforschungsbereich 195 (Universität Karlsruhe), and by a Grant from G.I.F., the German-Israeli Foundation for Scientific Research and Development.

[1] G. Sachs, W. Stöcklein, B. Bail, E. Dormann, and M. Schwoerer, Chem. Phys. Lett. **89**, 179 (1982).
[2] G. Sachs and E. Dormann, Synth. Metals **25**, 157 (1988).
[3] W. Hoeptner, M. Mehring, J. U. von Schütz, H. C. Wolf, B. S. Morra, V. Enkelmann, and G. Wegner, Chem. Phys. **73**, 253 (1982).
[4] G. G. Maresch, A. Grupp, M. Mehring, and J. U. von Schütz, and H. C. Wolf, J. Phys. **46**, 461 (1985).
[5] G. G. Maresch, A. Grupp, M. Mehring, and J. U. v. Schütz, Synth. Metals **16**, 161 (1986).
[6] G. Denninger, Adv. Solid State Phys. **30**, 113 (1990).
[7] R. Ruf, H. Lossau, and E. Dormann, Synth. Metals **70**, 1215 (1995).
[8] R. Ruf, N. Kaplan, and E. Dormann, Phys. Rev. Lett. **74**, 2122 (1995); **75**, 1237 (1995); **76**, 334 (1996).
[9] N. Kaplan, E. Dormann, R. Ruf, A. Coy, and P. T. Callaghan, Phys. Rev. B **52**, 16 385 (1995).
[10] H. Endres, H. J. Keller, B. Müller, and D. Schweitzer, Acta Crystallogr. C **41**, 607 (1985).
[11] M. Burggraf, H. Dragan, P. Gruner-Bauer, H. W. Helberg, W. F. Kuhs, G. Mattern, D. Müller, W. Wendl, A. Wolter, and E. Dormann, Z. Phys. B **96**, 439 (1995).
[12] W. Brütting and W. Riess, Acta Phys. Pol. **87**, 785 (1995).
[13] A. Wolter, M. Burggraf, H. Dragan, U. Fasol, E. Dormann, H. W. Helberg, and D. Müller, Synth. Metals **71**, 1957 (1995).
[14] A. Wolter, U. Fasol, R. Jäppelt, and E. Dormann, Phys. Rev. B (to be published).
[15] T. C. Farrar, *Pulse and Fourier Transform NMR* (Academic, New York, 1971).
[16] R. J. Elliot, Phys. Rev. **96**, 266 (1954).
[17] D. Jerome and H. J. Schultz, Adv. Phys. **31**, 299 (1982).
[18] A. Carrington and A. D. McLachlan, *Introduction to Magnetic Resonance* (Harper & Row, New York, 1969).
[19] G. Soda, D. Jerome, M. Weger, J. Alizon, J. Gallice, H. Robert, J. M. Fahre, and L. Giral, J. Phys. (Paris) **38**, 931 (1977).
[20] A. Wolter, Ph. D. Thesis, Universität Karlsruhe, 1995.
[21] G. Sachs, E. Pöhlmann, and E. Dormann, J. Magn. Magn. Mater. **69**, 131 (1987).
[22] E. Dormann and G. Sachs, Ber. Bunsenges. Phys. Chem. **91**, 879 (1987).
[23] H. C. Torrey, Phys. Rev. **104**, 563 (1956).
[24] P. T. Callaghan, A. Coy, E. Dormann, R. Ruf and N. Kaplan, J. Magn. Res. A **111**, 127 (1994).
[25] C. H. Neuman, J. Chem. Phys. **60**, 4508 (1974).
[26] B. Robertson, Phys. Rev. **151**, 273 (1966).
[27] S. D. Stoller, W. Happer and F. J. Dyson, Phys. Rev. A **44**, 7459 (1991).
[28] T. M. de Swiet and P. N. Sen, J. Chem. Phys. **100**, 5597 (1994).
[29] M. D. Hürlimann, K. G. Helmer, T. M. de Swiet, P. N. Sen, and C. H. Sotak, J. Magn. Res. A **113**, 260 (1995).
[30] K. H. Hellwege, *Einführung in die Festkörperphysik* (Springer-Verlag, Berlin, 1988).
[31] N. W. Ashcroft and N. D. Mermin, in *Solid State Physics* (Holt, Rinehart and Winston, New York, 1976).
[32] P. H. Nguyen, G. Paasch, W. Brütting, and W. Riess, Phys. Rev. B **49**, 5172 (1994).